

Comparison study of some finite volume and finite element methods for the shallow water equations with bottom topography and friction terms

M. Lukáčová - Medvidřová¹ and U. Teschke²

Abstract

We present a comparison of two discretization methods for the shallow water equations, namely the finite volume method and the finite element scheme. A reliable model for practical interests includes terms modelling the bottom topography as well as the friction effects. The resulting equations belong to the class of systems of hyperbolic partial differential equations of first order with zero order source terms, the so-called balance laws. In order to approximate correctly steady equilibrium states we need to derive a well-balanced approximation of the source term in the finite volume framework. As a result our finite volume method, a genuinely multidimensional finite volume evolution Galerkin (FVEG) scheme, approximates correctly steady states as well as their small perturbations (quasi-steady states). The second discretization scheme, which has been used for practical river flow simulations, is the finite element method (FEM). In contrary to the FVEG scheme, which is a time explicit scheme, the FEM uses an implicit time discretization and the Newton-Raphson iterative scheme for inner iterations. We show that both discretization techniques approximate correctly steady and quasi-steady states with bottom topography and friction and compare their accuracy and performance.

Key words: well-balanced schemes, steady states, systems of hyperbolic balance laws, shallow water equations, evolution Galerkin schemes, finite element schemes, Darcy-Weisbach friction law, Newton-Raphson method

AMS Subject Classification: 65L05, 65M06, 35L45, 35L65, 65M25, 65M15

1 Introduction

Description of natural river processes is very complex. The main aim is to determine the water level at a specific place and time. Reliable mathematical models as well as robust, fast and accurate numerical simulations are very important for predictions of floods and have large economical impact. One of the main difficulty of the reliable calculation is the determination of the friction which counteracts the river flows. Numerical simulation of

¹Institute of numerical simulations, Hamburg University of Technology, Schwarzenbergstraße 95, 21079 Hamburg, Germany, email: lukacova@tu-harburg.de

²IMS Ingenieurgesellschaft mbH, Stadtdeich 5, D 20097 Hamburg, Germany, email: ulf.teschke@ufz.de

natural river flows is based on the two-dimensional shallow water equations. The shallow water system consists of the continuity equation and the momentum equations

$$\frac{\partial \mathbf{u}}{\partial t} + \frac{\partial \mathbf{f}_1(\mathbf{u})}{\partial x} + \frac{\partial \mathbf{f}_2(\mathbf{u})}{\partial y} = \mathbf{b}(\mathbf{u}), \quad (1.1)$$

where

$$\mathbf{u} = \begin{pmatrix} h \\ hu \\ hv \end{pmatrix}, \quad \mathbf{f}_1(\mathbf{u}) = \begin{pmatrix} hu \\ hu^2 + \frac{1}{2}gh^2 \\ huv \end{pmatrix},$$

$$\mathbf{f}_2(\mathbf{u}) = \begin{pmatrix} hv \\ huv \\ hv^2 + \frac{1}{2}gh^2 \end{pmatrix}, \quad \mathbf{b}(\mathbf{u}) = \begin{pmatrix} 0 \\ -gh(\frac{\partial b}{\partial x} + S_{fx}) \\ -gh(\frac{\partial b}{\partial y} + S_{fy}) \end{pmatrix}.$$

Here $h = h(x, y)$ denotes the water depth, $u = u(x, y, t)$, $v = v(x, y, t)$ are vertically averaged velocity components in x - and y -direction, g stands for the gravitational constant, $b = b(x, y)$ denotes the bottom topography and S_{fx}, S_{fy} are the friction terms in x - and y - directions.

In practice even the one dimensional analogy of (1.1), the so-called Saint-Venant equations, are often used

$$\frac{\partial \mathbf{w}}{\partial t} + \frac{\partial \mathbf{f}_1(\mathbf{w})}{\partial x} = \mathbf{b}(\mathbf{w}), \quad (1.2)$$

where

$$\mathbf{w} = \begin{pmatrix} A \\ Q \end{pmatrix}, \quad \mathbf{f}_1(\mathbf{w}) = \begin{pmatrix} Q \\ Q^2/A \end{pmatrix}, \quad \mathbf{b}(\mathbf{w}) = \begin{pmatrix} 0 \\ -gA(\frac{\partial z}{\partial x} + S_{fx}) \end{pmatrix}.$$

Here $A = A(h(x, t), x)$ denotes the cross section area, $Q = Q(x, t) = Au$ is the discharge and $z = h + b$ stands for the water surface.

The determination of the friction slopes S_{fx}, S_{fy} is a very complex problem. The friction law for the river flow is often approximately modelled by the friction law of pipe flow, but the pipe flow is much simpler than natural river flow. In fact, the main difficulty of the evaluation of friction slope is the reflection of various characteristics of natural river flow into one parameter. Typical characteristics of natural rivers are:

- structured cross sectional area with mass and momentum exchange at the boundaries
- complex cross sectional area as a function of depth of water
- vegetation of different kind
- different roughness at the same cross sectional area
- meandering
- retention effects.

A good overview of the theory of friction slope in natural river flow can be found in [17] and the references therein. For one dimensional steady flow situation S_{fx} can be expressed by an integral relation

$$\rho g \int_{x_1}^{x_2} S_{fx} A(h(x), x) dx = \int_{A_{bot}} \tau_{bot}(x) dx dy . \quad (1.3)$$

The right hand side term describes a part of the weight of the fluid element with the cross section $A(x)$. Here τ_{bot} is the shear stress at the river bottom at the bottom area A_{bot} and x_1 and x_2 are the boundaries of the fluid element in the x -direction. The bottom composition of a river can vary rapidly, especially when vegetation is taken into account. In the literature several methods in order to determine the friction slope can be found, cf., e.g. [16] and [19]. Basis for our calculation is the friction law of Darcy-Weisbach. Thus, the friction slopes are calculated by, see, e.g. [17],

$$S_{fx}(h, u, v, x, y, t) = \frac{\lambda u \sqrt{u^2 + v^2}}{8g h} , \quad S_{fy}(h, u, v, x, y, t) = \frac{\lambda v \sqrt{u^2 + v^2}}{8g h} , \quad (1.4)$$

where λ stays for the so-called resistance value. This is determined according to the simplified form of the Colebrook-White relation

$$\frac{1}{\sqrt{\lambda}} = -2.03 \log \left(\frac{k_s/h}{14.84} \right) ,$$

which was originally found for pipe flow. In the case of one-dimensional flow the friction slope S_f is given in the analogy to (1.3) as

$$S_f(A, Q, x, t) = \frac{\lambda}{8gr_{hy}} \frac{|Q|Q}{A^2} , \quad \frac{1}{\sqrt{\lambda}} = -2.03 \log \left(\frac{k_s/r_{hy}}{14.84} \right) ,$$

where r_{hy} stays for the hydraulic radius. When the above listed characteristics of natural rivers have to be reflected more complex models for the resistance value λ are necessary. Here k_s denotes the Nikuradse grain roughness size, which depends on the composition of the river bottom, especially of the sediment size. Typically, k_s can vary from 1 mm for beton until 300 mm for bottom with dense vegetation, or sometimes in an even wider range.

One possible and simple way to solve a system of balance laws (1.1) or (1.2) is to apply the operator splitting approach and solve separately the resulting homogenous system of hyperbolic conservation laws, e.g. by using the finite volume or finite element method, and the system of ordinary differential equations, which includes the right-hand-side source terms. However, this can lead to the structural deficiencies and strong oscillations in the solutions, especially when steady solutions or their small perturbations are to be computed numerically. In fact, most of the geophysical flows, including river flows, are nearly steady flows, that are closed to the equilibrium states of the dynamical system (1.1). Consider a steady flow, i.e. we have for material derivatives $dh/dt = 0$, $du/dt = 0$, $dv/dt = 0$. In this case the rest of the gradient of fluxes is balanced with the right-hand side source term, which yields the following balance condition in the x -direction $\partial_x(gh^2/2) = -gh(\partial_x b + S_{fx})$. Assume that R is a primitive to S_{fx} . Then the balance

condition can be rewritten as $gh\partial_x(h + b + R) = 0$. An analogous condition holds in the y -direction. These *equilibrium conditions* yield the well-balanced approximation of the source term. The resulting schemes are called *the well-balanced schemes*, cf., e.g. [1], [4], [6], [8] and the references therein for other well-balanced schemes in literature.

Our aim is to study the approximation of steady equilibrium states for balance law (1.1), or (1.2), in the framework of the finite element as well as finite volume methods. In the case of the finite volume method we use a genuinely multidimensional finite volume evolution Galerkin scheme, which has been shown to perform very accurately in comparison to classical finite volume methods, e.g. dimensional splitting schemes, cf. [10], [11].

2 Finite element method

The finite element method is a well known method for solving differential equations. Numerous research and applications have shown good results in the area of structural as well as fluid mechanics. Our approach uses a formulation based on the method of weighted residuals to develop the discrete equations.

The method presented here has been used for practical applications in hydrology. Let q_e be the lateral inflow per unit length and β denote the momentum coefficient for flows with the velocity, which is not uniform, i.e.

$$\beta = \frac{A}{Q^2} \int_A u^2(y, z) dx dy . \quad (2.1)$$

Then the continuity equation (1.2)₁ is equivalent to

$$\frac{\partial A}{\partial t} + \frac{\partial Q}{\partial x} - q_e = 0 . \quad (2.2)$$

Applying the rule for derivation of fraction Q^2/A in (1.2)₂ we obtain the following formulation of the momentum equation, which is equivalent to (1.2)₂ for smooth solutions

$$\frac{\partial Q}{\partial t} + \frac{Q^2}{A} \frac{\partial \beta}{\partial x} + 2\beta \frac{Q}{A} \frac{\partial Q}{\partial x} - \beta \frac{Q^2}{A^2} \frac{\partial A}{\partial x} + gA \frac{\partial z}{\partial x} + gAS_f - q_e v_{ex} = 0 . \quad (2.3)$$

Here v_{ex} is the velocity component of the inflow in the x -direction. For the detailed derivation of (2.2) and (2.3) see [17].

The finite element approximation with the basis functions $N_i(x)$ for the independent variables h and Q gives

$$Q(x) = \sum_{i=1}^n Q_i N_i(x) , \quad h(x) = \sum_{i=1}^n h_i N_i(x) , \quad (2.4)$$

where i is the index of a node, n is the total number of nodes, h_i approximates the water depth and Q_i the discharge at the node i . The cross section $A(h, x)$ is a given function depending on h and x . The differential equations (2.2) and (2.3) are weighted with weighted functions (i.e. test functions) over the whole domain Ω yielding the following equations

$$G \equiv \int_{\Omega} W_i \left(\frac{\partial A}{\partial t} + \frac{\partial Q}{\partial x} - q_e \right) dx = 0 , \quad i = 1, 2, \dots, n , \quad (2.5)$$

$$F \equiv \int_{\Omega} W_i \left(\frac{\partial Q}{\partial t} + \frac{Q^2}{A} \frac{\partial \beta}{\partial x} + 2\beta \frac{Q}{A} \frac{\partial Q}{\partial x} - \beta \frac{Q^2}{A^2} \frac{\partial A}{\partial x} + gA \frac{\partial z}{\partial x} + gAS_f - q_e v_{ex} \right) dx = 0, \quad (2.6)$$

$i = 1, 2, \dots, n.$

We have chosen the weighted functions $W_i(x)$ to be the same functions as the basis function $N_i(x)$. Equations (2.5) and (2.6) represent the classical *Galerkin Method*.

2.1 Time integration scheme

In the time integration scheme we follow the approach of King [5]. The variation with time will be described by the following function

$$y(t) = a + bt + ct^\gamma \quad (2.7)$$

with a constant coefficient γ . It can be shown that the following equation

$$\frac{dy(t + \Delta t)}{dt} = \gamma \frac{y(t + \Delta t) - y(t)}{\Delta t} + (1 - \gamma) \frac{dy(t)}{dt} \quad (2.8)$$

holds [17]. In our numerical experiments for steady or quasi-steady, i.e. perturbed steady flows, we have tested several values of γ , $\gamma \in [1, 2]$, and found only marginal differences in accuracy as far as the method is stable. Therefore we set $\gamma = 1$. In this case the scheme reduces to the conventional linear integration scheme, i.e. the implicit Euler method. For $\gamma = 2$ the time discretization is formally second order and we get a semi-implicit scheme. Unfortunately, this choice yields an unstable scheme as we will show below.

2.2 Newton Raphson Procedure

Since the equations (2.5) and (2.6) are nonlinear we have used the Newton-Raphson procedure in order to solve them iteratively

$$\begin{bmatrix} \frac{\partial F_1}{\partial h_1} & \dots & \frac{\partial F_1}{\partial h_n} & \frac{\partial F_1}{\partial Q_1} & \dots & \frac{\partial F_1}{\partial Q_n} \\ \frac{\partial G_1}{\partial h_1} & \dots & \frac{\partial G_1}{\partial h_n} & \frac{\partial G_1}{\partial Q_1} & \dots & \frac{\partial G_1}{\partial Q_n} \\ \vdots & \ddots & \vdots & \vdots & \ddots & \vdots \\ \frac{\partial F_n}{\partial h_1} & \dots & \frac{\partial F_n}{\partial h_n} & \frac{\partial F_n}{\partial Q_1} & \dots & \frac{\partial F_n}{\partial Q_n} \\ \frac{\partial G_n}{\partial h_1} & \dots & \frac{\partial G_n}{\partial h_n} & \frac{\partial G_n}{\partial Q_1} & \dots & \frac{\partial G_n}{\partial Q_n} \end{bmatrix} \cdot \begin{bmatrix} (h_1^{new} - h_1^{old}) \\ \vdots \\ (h_n^{new} - h_n^{old}) \\ (Q_1^{new} - Q_1^{old}) \\ \vdots \\ (Q_n^{new} - Q_n^{old}) \end{bmatrix} + \begin{bmatrix} F_1 \\ G_1 \\ \vdots \\ \vdots \\ F_n \\ G_n \end{bmatrix} = \begin{bmatrix} 0 \\ 0 \\ \vdots \\ \vdots \\ 0 \\ 0 \end{bmatrix}. \quad (2.9)$$

Most of the derivatives in the Jacobian matrix are zeros, which is a consequence of the used basis functions, i.e. the Jacobian is a sparse matrix. Equations (2.9) have to be simplified further. The integrals F_1, \dots, F_n and G_1, \dots, G_n as well as their derivatives, cf. (6.2) - (6.6), have to be approximated by a suitable numerical integration. In our method we have used the Gauss quadrature rule with four points [5]. Let us point out that the resulting linear system has been solved here by means of the Gauss elimination. Actually, in typical practical problems arising in river flow industry the number of degrees of freedom is not very high and the Gauss elimination behaves reasonably with respect to time complexity, cf. [17]. However, for more precise computations yielding large algebraic systems suitable iterative methods should be used.

3 Finite volume evolution Galerkin method

In our recent works [9], [10], [11] we have proposed a new genuinely multidimensional finite volume evolution Galerkin method (FVEG), which is used to solve numerically nonlinear hyperbolic conservation laws. The method is based on the theory of bicharacteristics, which is combined with the finite volume framework. It can be also viewed as a predictor-corrector scheme; in the predictor step data are evolved along the bicharacteristics, or along the bicharacteristic cone, in order to determine approximate solution on cell interfaces. In the corrector step the finite volume update is done. Thus, in our finite volume method we do not use any one-dimensional approximate Riemann solver, instead the intermediate solution on cell interfaces is computed by means of an approximate evolution operator. The reader is referred to [3], [7], [14] and the references therein for other recent genuinely multidimensional methods.

To point out multidimensional features of the FVEG scheme we will give the description of the method for two-dimensional situations. Our computational domain Ω will be divided into a finite number of regular finite volumes $\Omega_{ij} = [x_{i-\frac{1}{2}}, x_{i+\frac{1}{2}}] \times [y_{j-\frac{1}{2}}, y_{j+\frac{1}{2}}] = [x_i - \hbar/2, x_i + \hbar/2] \times [y_j - \hbar/2, y_j + \hbar/2]$, $i, j \in \mathbb{Z}$, \hbar is a mesh step. Further, we denote by \mathbf{U}_{ij}^n the piecewise constant approximate solution on a mesh cell Ω_{ij} at time t_n and start with initial approximations obtained by the integral averages $\mathbf{U}_{ij}^0 = \int_{\Omega_{ij}} \mathbf{U}(\cdot, 0)$. The finite volume evolution Galerkin scheme can be formulated as follows

$$\mathbf{U}^{n+1} = \mathbf{U}^n - \frac{\Delta t}{\hbar} \sum_{k=1}^2 \delta_{x_k} \bar{\mathbf{f}}_k^{n+1/2} + \mathbf{B}^{n+1/2}, \quad (3.1)$$

where Δt is a time step, δ_{x_k} stays for the central difference operator in the x_k -direction, $k = 1, 2$, and $\bar{\mathbf{f}}_k^{n+1/2}$ represents an approximation to the edge flux at the intermediate time level $t_n + \Delta t/2$. Further $\mathbf{B}^{n+1/2}$ stands for the approximation of the source term \mathbf{b} . The cell interface fluxes $\bar{\mathbf{f}}_k^{n+1/2}$ are evolved using an approximate evolution operator denoted by $E_{\Delta t/2}$ to $t_n + \Delta t/2$ and averaged along the cell interface edge denoted by \mathcal{E} , i.e.

$$\bar{\mathbf{f}}_k^{n+1/2} := \frac{1}{\hbar} \int_{\mathcal{E}} \mathbf{f}_k(E_{\Delta t/2} \mathbf{U}^n) dS. \quad (3.2)$$

The well-balanced approximate evolution operator $E_{\Delta t/2}$ for system (1.1) will be given in the Section 3.2.

3.1 A well-balanced approximation of the source terms in the finite volume update

As already mentioned above we want to approximate source terms in the finite volume update in such a way that the balance between the source terms and the gradient of fluxes will be exactly preserved. This can be done by approximating the source term by using its values on interfaces, cf. [15].

Let us consider a steady flow,

$$\begin{aligned} \frac{du}{dt} &\equiv \frac{\partial u}{\partial t} + u \frac{\partial u}{\partial x} + v \frac{\partial u}{\partial y} = 0, & \frac{dv}{dt} &= 0, & \frac{dh}{dt} &= 0, \\ gh \frac{\partial(h+b+R)}{\partial x} &= 0, & gh \frac{\partial(h+b+T)}{\partial y} &= 0, \end{aligned} \quad (3.3)$$

where R and T are primitives to S_{fx} and S_{fy} , respectively. Note that the stationary state, the so-called lake at rest, i.e. $u = 0 = v$, and $h+b = \text{const.}$, is a special equilibrium state, that is included here.

Assume that (3.3) holds, then the second equation of (3.1) yields

$$\begin{aligned} \frac{g}{2\bar{h}^2} \int_{y_{i-1/2}}^{y_{i+1/2}} \left((h_{i+1/2}^{n+1/2})^2 - (h_{i-1/2}^{n+1/2})^2 \right) dS_y \\ = \frac{g}{2\bar{h}^2} \int_{y_{i-1/2}}^{y_{i+1/2}} \left(h_{i+1/2}^{n+1/2} + h_{i-1/2}^{n+1/2} \right) \left(h_{i+1/2}^{n+1/2} - h_{i-1/2}^{n+1/2} \right) dS_y. \end{aligned} \quad (3.4)$$

This and the equilibrium condition $gh\partial_x(h+b+R) = 0$ imply the well-balanced approximation of the source term

$$\begin{aligned} \frac{1}{\bar{h}^2} \int_{\Omega_{ij}} B_2(\mathbf{U}^{n+1/2}) &= \frac{1}{\bar{h}^2} \int_{x_{i-1/2}}^{x_{i+1/2}} \int_{y_{i-1/2}}^{y_{i+1/2}} -gh^{n+1/2} (\partial_x b^{n+1/2} + \partial_x R^{n+1/2}) \\ &\approx \frac{-g}{\bar{h}} \int_{y_{i-1/2}}^{y_{i+1/2}} \frac{h_{i+1/2}^{n+1/2} + h_{i-1/2}^{n+1/2}}{2} \frac{(b_{i+1/2} + R_{i+1/2}^{n+1/2}) - (b_{i-1/2} + R_{i-1/2}^{n+1/2})}{\bar{h}} dS_y. \end{aligned}$$

Integrals along vertical cell interfaces are approximated by the Simpson rule similarly to the cell interface integration used in (3.4). An analogous approximation of the source term is used also in the third equation for the y - direction.

3.2 Well-balanced approximate evolution operator

In order to evaluate fluxes on cell interfaces we need to derive an approximate evolution operator which gives suitable time approximation of the exact integral equations that are implicit in time. The exact integral equations describe time evolution of the solution to the linearized system and can be obtained by exploring the hyperbolic structure of the shallow water system (1.1) and applying the theory of bicharacteristics, cf. [2], [9, 10, 11]. In [12] the well-balanced approximate evolution operators for the shallow water equations with bottom topography have been derived. The friction terms will be approximated in an analogous way as the Coriolis forces in [13]. We have shown in [13] that these operators preserve stationary equilibrium states, i.e. $u = 0 = v$, $z = h+b = \text{const.}$ as well as steady flows.

The well-balanced approximate evolution operator E_{Δ}^{const} for piecewise constant data reads

$$\begin{aligned}
h(P) &= -b(P) + \frac{1}{2\pi} \int_0^{2\pi} (h(Q) + b(Q)) - \frac{\tilde{c}}{g} u(Q) \operatorname{sgn}(\cos \theta) - \frac{\tilde{c}}{g} v(Q) \operatorname{sgn}(\sin \theta) d\theta \\
&\quad + O(\Delta t^2), \\
u(P) &= \frac{1}{2\pi} \int_0^{2\pi} -\frac{g}{\tilde{c}} (h(Q) + b(Q) + R(Q)) \operatorname{sgn}(\cos \theta) + u(Q) \left(\cos^2 \theta + \frac{1}{2} \right) \\
&\quad + v(Q) \sin \theta \cos \theta d\theta + O(\Delta t^2), \\
v(P) &= \frac{1}{2\pi} \int_0^{2\pi} -\frac{g}{\tilde{c}} (h(Q) + b(Q) + T(Q)) \operatorname{sgn}(\sin \theta) + u(Q) (\sin \theta \cos \theta) \\
&\quad + v(Q) \left(\sin^2 \theta + \frac{1}{2} \right) d\theta + O(\Delta t^2).
\end{aligned} \tag{3.5}$$

If the continuous piecewise bilinear data are used the well-balanced approximate evolution operator, which is denoted by E_{Δ}^{bilin} , reads

$$\begin{aligned}
h(P) &= -b(P) + (h(Q_0) - b(Q_0)) + \frac{1}{4} \int_0^{2\pi} ((h(Q) - h(Q_0)) + (b(Q) - b(Q_0))) d\theta \\
&\quad - \frac{1}{\pi} \int_0^{2\pi} \left(\frac{\tilde{c}}{g} u(Q) \cos \theta + \frac{\tilde{c}}{g} v(Q) \sin \theta \right) d\theta + O(\Delta t^2), \\
u(P) &= u(Q_0) - \frac{1}{\pi} \int_0^{2\pi} \frac{g}{\tilde{c}} (h(Q) + b(Q) + R(Q)) \cos \theta d\theta \\
&\quad + \frac{1}{4} \int_0^{2\pi} \left(3u(Q) \cos^2 \theta + 3v(Q) \sin \theta \cos \theta - u(Q) - \frac{1}{2} u(Q_0) \right) d\theta \\
&\quad + O(\Delta t^2), \\
v(P) &= v(Q_0) - \frac{1}{\pi} \int_0^{2\pi} \frac{g}{\tilde{c}} (h(Q) + b(Q) + T(Q)) \sin \theta d\theta \\
&\quad + \frac{1}{4} \int_0^{2\pi} \left(3u(Q) \sin \theta \cos \theta + 3v(Q) \sin^2 \theta - v(Q) - \frac{1}{2} v(Q_0) \right) d\theta \\
&\quad + O(\Delta t^2).
\end{aligned} \tag{3.6}$$

The approximate evolution operators (3.5) and (3.6) are used in (3.2) in order to evolve fluxes along cell interfaces. Thus, the first order method is obtained using the approximate evolution operator E_{Δ}^{const}

$$\bar{\mathbf{f}}_k^{n+1/2} = \frac{1}{h} \int_{\mathcal{E}} \mathbf{f}_k(E_{\Delta t/2}^{const} \mathbf{U}^n) dS, \quad k = 1, 2,$$

whereas in the second order FVEG scheme a suitable combination of the approximate evolution operator E_{Δ}^{bilin} and E_{Δ}^{const} is used. We apply E_{Δ}^{bilin} to evolve slopes and E_{Δ}^{const} to evolve the corresponding constant part in order to preserve conservativity

$$\bar{\mathbf{f}}_k^{n+1/2} = \frac{1}{\bar{h}} \int_{\mathcal{E}} \mathbf{f}_k \left(E_{\Delta t/2}^{bilin} R_h \mathbf{U}^n + E_{\Delta t/2}^{const} (1 - \mu_x^2 \mu_y^2) \mathbf{U}^n \right) dS.$$

Here $R_h \mathbf{U}$ denotes a continuous bilinear recovery and $\mu_x^2 U_{ij} = 1/4(U_{i+1,j} + 2U_{ij} + U_{i-1,j})$; an analogous notation is used for the y -direction.

4 Numerical experiments

In this section we compare the behavior of both FEM and FVEG schemes through several test problems.

Example 1: channel flow with friction

In this example we simulate a steady uniform flow in a regular rectangular channel of $\ell = 1 \text{ km}$ length and $w = 6 \text{ m}$ width. The bottom profile is given by

$$b(x, y) = -0.001x + 1 \quad 0 < x < 1000, \quad y \in [0, 6].$$

For the FVEG method the initial data are chosen as a stationary state

$$h(x, y, 0) + b(x, y) = 2, \quad u(x, y, 0) = 0 = v(x, y, 0).$$

At the inflow, i.e. $x = 0 \text{ m}$, the volume rate flow is taken to be $Q \equiv w h u = 3 \text{ m}^3 \text{ s}^{-1}$. The inflow velocity in the y -direction is 0 m s^{-1} . At the outflow, i.e. $x = 1000 \text{ m}$, we have imposed for the FVEG method absorbing boundary conditions by extrapolating the data in the outer normal direction. We have tested several friction parameters of the bottom, $k_s = 0.1, 0.2$ and 0.3 m . In order to evaluate friction slopes the hydraulic radius r_{hy} is to be computed. For a regular rectangular channel it is computed by the formula $r_{hy} = w h / (2h + b)$.

Solutions computed by the FVEG method is evolved in time until the steady equilibrium state is achieved, i.e. until $\|h^{n+1} - h^n\| \leq 10^{-8}$. Since the FVEG method is explicit in time, the CFL stability condition needs to be satisfied. We set CFL number to 0.8 in all our experiments. The FVEG method (3.1) solves two-dimensional shallow water equations (1.1), the solution in the y -direction is constant.

The FEM computes directly solution of the stationary equations, i.e. $\frac{\partial \mathbf{w}}{\partial t} = 0$ in (1.2), i.e. (2.2) and (2.3). The FEM method (2.5), (2.6) approximates the one-dimensional Saint-Venant equations (1.2), i.e. (2.2), (2.3). The comparisons of the shallow water depths are given for different values of k_s in the Table 1. The results indicate clearly very good agreement of both methods, the second order FVEG scheme as well as FEM.

$k_s[m]$	$h[m]$	
	FEM	FVEG
0.1	0.6395567	0.640179
0.2	0.7113167	0.712090
0.3	0.7626931	0.763592

Table 1: Comparison of water depths for a steady flow with different friction parameters for the bottom.

Example 2: channel flow with friction and varied topography

In this example we simulate again a steady flow in a channel having a varying bottom topography. We take a non smooth bottom having discontinuity in the first derivative, the profile is given as

$$b(x, y) = \begin{cases} -0.001(x - 500) + 0.5 & \text{if } 0 < x < 500, y \in [0, 6], \\ 0.5 & \text{if } 500 < x < 1000, y \in [0, 6]. \end{cases}$$

The length of the channel is $\ell = 1 \text{ km}$ and width is $w = 6 \text{ m}$. The grain roughness size parameter of the bottom is set to $k_s = 0.1 \text{ m}$. We take again for the FVEG a stationary state as the initial data, i.e. $h(x, y, 0) + b(x, y) = 2$, $u(x, y, 0) = 0 = v(x, y, 0)$. Other parameters, inflow and outflow boundary conditions, are the same as in the previous experiment. The solution is evolved in time until a steady state is obtained. Our steady state solutions obtained by different methods, i.e. the FVEG method as well as the FEM are in a very good agreement, see Figures 1. No singular corner effects on smoothness of the solution can be noticed.

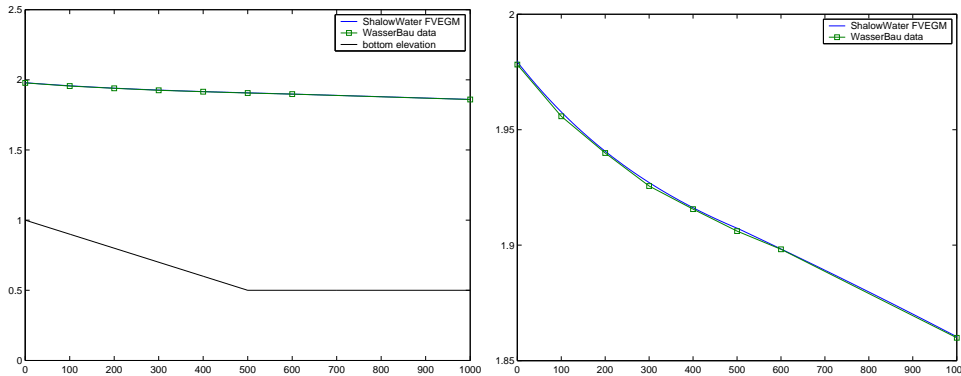


Figure 1: Comparison of the two-dimensional solution of water depth h obtained by the FVEG scheme (solid line) and the one-dimensional steady solution obtained by the FEM scheme (boxes).

Example 3: propagating waves with bottom topography

In this example small perturbations of a stationary flow are simulated. It is well-known that this is a hard test for methods which do not take care on a well-balanced approximation of the bottom topography and friction terms. In this case strong oscillations can

appear in solutions as soon as small perturbations propagate over topographical changes. We consider here a problem analogous to that proposed by LeVeque, cf.[8]. The bottom topography consists of one hump

$$b(x) = \begin{cases} 0.5(\cos(\pi(x - 50)/10) + 0.5) & \text{if } |x - 50| < 10 \\ 0 & \text{otherwise} \end{cases}$$

and the initial data are $u(x, 0) = 0$,

$$h(x, 0) = \begin{cases} 2 - b(x) + \varepsilon & \text{if } 10 < x < 20 \\ 2 - b(x) & \text{otherwise.} \end{cases}$$

The parameter ε is chosen to be 0.2 and 0.02. The computational domain is $[0, 100]$. The reflection boundary conditions, i.e. fixed wall conditions, have been imposed on $x = 0$ m and $x = 100$ m. In the FEM the Dirichlet boundary conditions, i.e. $Q = 0$, are imposed, which is an alternative to model fixed walls. The value of k_s is set to 0.1 m.

Firstly the perturbation parameter is taken to be $\varepsilon = 0.2$. In Figures 2,3,4 we can see propagation of small perturbations of the water depth h for different times until $t = 19$ seconds. Solution is computed on a mesh with 500 cells with the second order FVEG method as well as FEM.

The FVEG method uses a time step Δt computed directly according to the CFL condition, $CFL = 0.8$. In the FEM time step Δt was set to $\Delta t = 0.015$ for $\varepsilon = 0.2$ and $\Delta t = 0.02$ for $\varepsilon = 0.02$. For $\varepsilon = 0.02$ the time step is of the same order as the time step used by the FVEG method. In the case $\varepsilon = 0.2$ the time step given automatically by the CFL condition is $\Delta t \approx 0.18$. In this case we have decided to suppress the time step for the FEM in order to reduce its numerical diffusion; as mentioned above $\Delta t = 0.02$ was used. In our numerical experiments we have seen that it was enough to take approximately 10 inner iterations in the Newton-Raphson method.

In Figure 5,6,7 the perturbation parameter is $\varepsilon = 0.02$, which is of the order of the discretization error being $O(10^{-2})$. We can notice correct resolution of small perturbations of the steady state by both methods even if the perturbations are of the order of the truncation error. Small initial oscillations can be noticed in the FEM, which is also slightly more dissipative than FVEG scheme. Since the flow is relatively slow, the Froude number is less than 1, no upwinding technique was necessary in the FEM. It would be however important to stabilize the finite element approximation by some type of upwinding technique or streamline diffusion technique, if flows with higher Froude numbers will be modelled. The FVEG method is constructing in such a way that it exactly balances influence of fluxes and the source terms. Although we have used just standard finite element approximation in the case of our FEM method, presented in the Chapter 2, no unbalanced oscillations can be noticed as perturbed waves propagate over the bottom topography even for small perturbations. The reason is the formulation (2.3) where we have modelled the water level z , instead of separating height h and topography b . Note also that the FEM discretizes also the friction term in the same way as the water level z . Thus the equilibrium condition (3.3) is preserved here as well.

For a two-dimensional analogy of this experiment similar results have been obtained by the FVEG method, cf. [13], which is a truly multidimensional scheme. The approach presented here, which is based on the FEM, is designed only for one-dimensional shallow flows, i.e. Saint Venant equations (2.2), (2.3). The generalization to fully two-dimensional case is possible as well. In practice the one-dimensional FEM computation of nearly one-

dimensional river flows are often satisfactory and moreover more effective and less time consuming.

Example 4: accuracy and performance

In this experiment we compare accuracy and computational time of both the FVEG and FE methods. First, we test the experimental order of convergence for a smooth solution. We consider the same geometry as in the previous Example 3 and take a smooth initial data:

$$h(x, 0) = \begin{cases} 2 - b(x) + \varepsilon \cos(\pi(x - 15)/10) & \text{if } 10 < x < 20 \\ 2 - b(x) & \text{otherwise,} \end{cases} \quad (4.1)$$

$$u(x, 0) = 0. \quad (4.2)$$

In order to reduce effects of boundary conditions we have used periodic boundary conditions. Although an exact solution is not known, we can still study the experimental order of convergence (EOC). This is computed in the following way using three meshes of sizes $N_1, N_2 := N_1/2, N_3 := N_2/2$, respectively

$$\text{EOC} = \log_2 \frac{\|U_{N_2}^n - U_{N_3}^n\|}{\|U_{N_1}^n - U_{N_2}^n\|}.$$

Here U_N^n is the approximate solution on the mesh with $N \times N$ cells at time step t_n . The computational domain $[0, 100]$ was consecutively divided into 20, 40, ..., 640 mesh cells. It should be pointed out that this one-dimensional problem was actually computed by the two-dimensional FVEG scheme on a domain $[0, 100] \times [0, 1]$ by imposing the tangential velocity $v = 0$. Discrete errors are evaluated on a half of the computational domain, i.e. for $x \in [25, 75]$. The final time was taken to be $t = 2$, parameter $\varepsilon = 0.2$, the friction parameter $k_s = 0.1m$ and CFL=0.8. The following three tables show the experimental order of convergence computed in the L^1 norms, analogous results have been obtained for the L^2 errors¹.

Table 2 demonstrates clearly the second order convergence of the FVEG scheme, which is consistent with theoretical investigations in [10]. See also [13] for further details on analysis of the FVEG scheme for hyperbolic balance laws.

For the FEM with parameter $\gamma = 1$, cf. (2.7), (2.8), the order is clearly one, due to the first order time approximation, see Table 3. We have obtained analogous results for $\gamma = 1.5$, which is a parameter oft used in practical engineering computations, cf. [5], [17]. In Table 4 we see a lost of the accuracy for the FEM with the parameter $\gamma = 2$, which indicates instability and would be seen more clearly on a finer mesh or for longer

¹We work here with the discrete norms defined in the usual way. Assume that U_N is a piecewise linear function on a mesh with N cells. Then

$$\|U_N\|_{L^q} := \left(\sum_{i=1}^N \int_{x_{i-1/2}}^{x_{i+1/2}} |U_N(x)|^q \right)^{1/q}, \quad q \in \mathbb{Z}, q \geq 1.$$

The integral on each mesh cell $[x_{i-1/2}, x_{i+1/2}]$ can be computed exactly or by a suitable numerical quadrature. For example, the midpoint or the trapezoidal rule suffice for the second order EOC tests using the L^2 norm. In the case of the discrete L^1 norm we have evaluated the cell integrals exactly since the absolute value is a non-smooth function, which can have a possible singularity within the mesh cell. Thus, the classical quadrature rules do not apply anymore.

computations. In order to illustrate the instability behaviour of FEM for $\gamma = 2$ we have used for this experiment a fixed $\Delta t = 0.02$, which is always below a time step $\Delta t \approx 0.18$ dictated by the CFL stability condition for CFL=0.8. This point should be investigated in future in more details, it would be desirable to have both the second order accuracy as well as stability for the FE approach.

Table 2: FVEG scheme: Convergence in the L^1 norm.

N	$\ h_{N/2}^n - h_N^n\ $	EOC	$\ u_{N/2}^n - u_N^n\ $	EOC
20	1.798e-003		1.819e-002	
40	2.091e-002	-	8.779e-003	1.0510
80	5.151e-003	2.0213	1.437e-003	2.6109
160	1.273e-003	2.0166	4.701e-004	1.6123
320	3.20e-004	1.9921	9.60e-005	2.2916
640	8.10e-005	1.9821	2.40e-005	2.0000

Table 3: FEM ($\gamma = 1$): Convergence in the L^1 norm.

N	$\ h_{N/2}^n - h_N^n\ $	EOC	$\ u_{N/2}^n - u_N^n\ $	EOC
20	1.2391e-002		2.2149e-002	
40	2.4786e-002	-	1.6170e-002	0.4539
80	8.0255e-003	1.6269	8.4591e-003	0.9348
160	2.4713e-003	1.6994	4.2324e-003	0.9990
320	1.0268e-003	1.2671	2.1488e-003	0.9779
640	4.8403e-004	1.0849	1.0821e-003	0.9897

In Table 5 we compare the computational efficiency of both numerical scheme. The results were obtained with a personal computer having 3,06 GHz Pentium 4 processor and 1,5 GB RAM. Figure 8 illustrates the CPU/accuracy behaviour graphically. We use the logarithmic scale on x -, y - axis. On the y - axis the sum of L^1 relative errors in both components h and u is depicted. We should point out that no attempt has been made in order to optimize the codes with respect to its CPU performance. We can notice that for practical meshes of about 80 to 160 mesh points the FVEG method is about 5 to 10 times faster yielding approximately 2.5 to 4 times smaller relative error than the FEM. In fact, the FEM code was written for general industrial applications and might behave not optimal here. For example, one can include some iteration method for solving the linear algebraic system in the FEM instead of the Gauss elimination, which might be too much time consuming as we are approaching fine meshes. Moreover, it is clear that concerning the accuracy the second order FVEG method clearly should overcome the first order FE scheme.

Table 4: FEM ($\gamma = 2$): Convergence in the L^1 norm.

N	$\ h_{N/2}^n - h_N^n\ $	EOC	$\ u_{N/2}^n - u_N^n\ $	EOC
20	1.311e-002		2.5916e-002	
40	2.6245e-002	-	2.0578e-002	0.3327
80	9.4017e-003	1.4806	1.4343e-002	0.5208
160	4.7951e-003	0.9714	7.3215e-003	0.9701
320	2.8851e-003	0.7329	5.9924e-003	0.2890
640	2.1097e-003	0.4515	4.3990e-003	0.4459

Table 5: CPU times for the FVEGM and FEM on meshes with N cells.

N	FVEGM	FEM
10	0.031 s	0.22 s
20	0.093 s	0.47 s
40	0.235 s	0.94 s
80	0.469 s	2.25 s
160	0.86 s	10.39 s
320	1.61 s	1 min. 23.6 s
640	3.93 s	17 min. 43.15 s

5 Concluding remarks

In the present paper we have compared two different discretization techniques for approximation of the system of shallow water equations with bottom topography terms and friction terms. The first method, the FEM, is based on a classical finite element approach using conforming linear finite elements for approximation of water depth h and for the volume rate Q . Discretization in time is done by the backward Euler scheme yielding the implicit finite difference scheme in time. We have illustrated that a formal second order time discretization yields an unstable scheme. In future a stable fully second order FEM discretization should be studied. The resulting nonlinear system of algebraic differential equations is solved iteratively by the Newton Raphson method. It should be pointed out that the presented scheme has already been used successfully for real river flow calculations in practice.

The second method, the finite volume evolution Galerkin method (FVEG), belongs to the class of multidimensional finite volume methods and it is a genuinely multidimensional variant of classical finite volume schemes. Thus, the FVEG method is a time explicit scheme and it resolves correctly also strong (multidimensional) shocks due to its upwinding character, cf. [9], [10], [11]. In order to obtain a higher order resolution a recovery step is included in the computation of cell interface fluxes. It should be pointed out that in contrast to the finite element scheme, the FVEG method uses discontinuous (bi-)linear discrete functions. Thus, the FEM as well as the FVEG scheme are second order accurate in space.

In order to resolve correctly steady equilibrium states a special, the so-called well-balanced, approximation of terms modelling the bottom topography as well as the friction effects was necessary. The FEM approximates these terms directly in the same way as other momentum terms and no special approximation was implemented. Both principally different discretization schemes have been extensively tested on various one-dimensional test problems, the representative choice of them is presented here. We have found in all our experiments a good agreement of both methods. Only relatively marginal differences can be found even on hard well-balanced problems, cf. Example 3. As far as the CPU time concerns we have found that the time explicit FVEG scheme was generally faster than the implicit FEM. Moreover, the FVEG scheme is second order in time as well as in space and thus it performs more efficiently than the FEM, cf. Figure 8. However, the CPU-efficiency needs to be considered relatively since it depends on the optimality and robustness of a code. We think that our comparative study can initiate an interest of engineers, who deal with the river flow simulations, to use new modern methods coming from other fields.

It is fair to mention that we have not yet dealt with other interesting problems like the resonance phenomenon and roll waves. In the case of resonance phenomenon two eigenvalues of the propagation matrix (Jacobian matrix) collapse. In the shallow water system with topography the resonance phenomenon appears when speed of gravity waves vanishes. Assume for example a decreasing topography, then the fluvial (subcritical) flow can change to the torrential (supercritical) flow through a stationary shock, the so-called hydraulic jump, the Bernoulli's law can be violated and the uniqueness of the weak entropy solution is lost.

Further, it is known that roll waves can occur in a uniform open-channel flow down an incline, when the Froude number is larger than two. It has been shown by [18] that the initial value problem for the Saint-Venant system including topography and friction is then linearly unstable. For steep channels the uniform flow can break to a series of waves or bores that are separated by smooth flow in a staircase pattern. These are the roll waves, i.e. discontinuous periodic travelling waves. The reliable and robust numerical schemes should produce correct approximations of these complex situations, too. This is a topic for further study.

6 Appendix

For the Newton-Raphson scheme equations (2.5) and (2.6) has to be differentiated. The corresponding derivatives, which are the entries of the Jacobian matrix in (2.9) are for each node $i = 1, \dots, n$:

$$\frac{\partial G}{\partial Q_i} = \int_0^L N^T \left(\frac{dN_i}{dx} \right) dx, \quad (6.1)$$

$$\frac{\partial G}{\partial h_i} = \int_0^L N^T N_i \left(\frac{\partial^2 A}{\partial h^2} \frac{\partial h}{\partial t} + \frac{\partial A}{\partial h} \frac{\gamma}{\Delta t} \right) dx, \quad (6.2)$$

$$\frac{\partial S_f}{\partial h_i} = -2N_i \frac{S_E Q^2}{Q_{Sch}^3} \left(\frac{\partial Q_{Sch}}{\partial h} \right), \quad (6.3)$$

$$\frac{\partial F}{\partial Q_i} = \int_0^L N^T N_i \left(\frac{\gamma}{\Delta t} + \frac{2Q}{A} \frac{\partial \beta}{\partial x} + \frac{2\beta}{A} \left(\frac{\partial Q}{\partial x} + \frac{Q}{N_i} \frac{\partial N_i}{\partial x} \right) - 2 \frac{\beta Q}{A^2} \frac{\partial A}{\partial x} + 2g \frac{A}{Q} S_f \right) dx. \quad (6.4)$$

Here Q_{Sch} describes the stage flow relationship for each cross section for steady uniform flow with the bottom slope S_E . In the described model we have approximated this relationship by polynomials in a preprocessing process. If there is no discharge $Q = 0$ than the last term of (6.4) vanishes, i.e.

$$2g \frac{A}{Q} S_f = 0, \quad (6.5)$$

for more details see [17].

$$\begin{aligned} \frac{\partial F}{\partial h_i} = \int_0^L \left\{ N^T \left[N_i \frac{Q^2}{A^2} \left(A \frac{\partial^2 \beta}{\partial h \partial x} - \frac{\partial \beta}{\partial x} \frac{\partial A}{\partial x} \right) + N_i \frac{2Q}{A^2} \frac{\partial Q}{\partial x} \left(A \frac{\partial \beta}{\partial h} - \beta \frac{\partial A}{\partial h} \right) \right. \right. \\ \left. \left. - N_i \frac{Q^2}{A^2} \left(\frac{\partial \beta}{\partial h} \frac{\partial A}{\partial x} + \beta \frac{\partial^2 A}{\partial h \partial x} - 2 \frac{\beta}{A} \frac{\partial A}{\partial h} \frac{\partial A}{\partial x} \right) \right. \right. \\ \left. \left. + g \left(N_i \frac{\partial A}{\partial h} \frac{\partial h}{\partial x} + A \frac{\partial N_i}{\partial x} \right) + g N_i \left(S_f \frac{\partial A}{\partial h} + A \frac{\partial S_f}{\partial h} \right) - g N_i S_0 \left(\frac{\partial A}{\partial h} \right) \right] \right\} dx \end{aligned} \quad (6.6)$$

In the examples presented in the paper the momentum coefficient β was set to unity and no lateral inflow q_e was considered.

We would like to point out that for arbitrary cross sections A the following relationship is often used

$$\frac{\partial A}{\partial h_i} = N_i(x) \frac{\partial A}{\partial h}, \quad (6.7)$$

see [17] for more detailed discussion.

Acknowledgements

This research was partially supported by the Graduate College ‘Conservation principles in the modelling and simulation of marine, atmospheric and technical systems’ of Deutsche Forschungsgemeinschaft as well as by the German Academic Exchange Service (DAAD). The first author would like to thank Erik Pasche, TU Hamburg-Harburg, for initiating this cooperation.

This paper has been finished during the sabbatical stay of the first author at the CSCAMM, University of Maryland. She would like to thank Eitan Tadmor, University of Maryland, for his generous support.

References

- [1] N. BOTTA, R. KLEIN, S. LANGENBERG, S. LÜTZENKIRCHEN, *Well balanced finite volume methods for nearly hydrostatic flows*, J. Comp. Phys., 196(2004), pp. 539-565.

- [2] R. COURANT, D. HILBERT, *Methoden der mathematischen Physik II*, second edition, Springer, Berlin, 1968
- [3] M. FEY, *Multidimensional upwinding, Part II. Decomposition of the Euler equations into advection equations*, J. Comp. Phys., 143(1998), pp. 181-199.
- [4] J.M. GREENBERG, A.-Y. LEROUX, *A well-balanced scheme for numerical processing of source terms in hyperbolic equations*, SIAM J. Numer. Anal., 33(1996), pp. 1-16.
- [5] I. KING, *Finite element models for unsteady flow routing through irregular channels*, Proc. first int. conference on FE in Waterresources, Pentech Press, London,(1976), pp. 166-184.
- [6] A. KURGANOV, D. LEVY, *Central-upwind schemes for the Saint-Venant system*, M²AN, Math. Model. Numer. Anal., 36(3)(2002), pp. 397-425.
- [7] R.J. LEVEQUE, *Wave propagation algorithms for multidimensional hyperbolic systems*, J. Comp. Phys., 1997(131), pp. 327-353.
- [8] R.J. LEVEQUE, *Balancing source terms and flux gradients in high-resolution Godunov methods: The quasi-steady wave propagation algorithm*, J. Comp. Phys., 146(1998), pp. 346-365.
- [9] M. LUKÁČOVÁ-MEDVIĐOVÁ, J. SAIBERTOVÁ, *Genuinely multidimensional evolution Galerkin schemes for the shallow water equations*, Enumath Conference, in Numerical Mathematics and Advanced Applications, F. Brezzi et al., eds., World Scientific Publishing Company, Singapore, 2002, pp. 105-114.
- [10] M. LUKÁČOVÁ-MEDVIĐOVÁ, J. SAIBERTOVÁ, G. WARNECKE, *Finite volume evolution Galerkin methods for nonlinear hyperbolic systems*, J. Comp. Phys., 183(2002), pp. 533-562.
- [11] M. LUKÁČOVÁ-MEDVIĐOVÁ, K.W. MORTON, G. WARNECKE, *Finite volume evolution Galerkin methods for hyperbolic problems*, SIAM J. Sci. Comput. 26(1)(2004), pp. 1-30.
- [12] M. LUKÁČOVÁ-MEDVIĐOVÁ, Z. VLK, *Well-balanced finite volume evolution Galerkin methods for the shallow water equations with source terms*, Int. J. Numer. Meth. Fluids 47(10-11)(2005), pp. 1165-1171.
- [13] M. LUKÁČOVÁ-MEDVIĐOVÁ, S. NOELLE, M. KRAFT, *Well-balanced finite volume evolution Galerkin methods for the shallow water equations*, submitted to J. Comp. Phys., 2005.
- [14] S. NOELLE, *The MOT-ICE: a new high-resolution wave-propagation algorithm for multidimensional systems of conservative laws based on Fey's method of transport*, J. Comp. Phys. 164(2000), pp. 283-334.
- [15] J. SHI, *A steady-state capturing method for hyperbolic systems with geometrical source terms*, M²AN, Math. Model. Numer. Anal., 35(4)(2001), pp. 631-646.

- [16] U. TESCHKE, *A new procedure of solving the one-dimensional Saint-Venant equations for natural rivers*, in *Wasserbau fünf Jahre*, E.Pasche, ed., TU Hamburg-Harburg, 2003, pp. 35-39.
- [17] U. TESCHKE, *Zur Berechnung eindimensionaler instationärer Strömungen von natürlichen Fließgewässern mit der Methode der Finiten Elemente*, PhD Dissertation TU Hamburg-Harburg, 2003, Fortschritt-Berichte VDI, 7/ 458, 2004.
- [18] J. WHITHAM, *Linear and Nonlinear Waves*, Wiley, 1974.
- [19] B.C. YEN, *Open channel flow resistance*, *J. Hydraulic Eng.* 128(2002), pp. 20-39

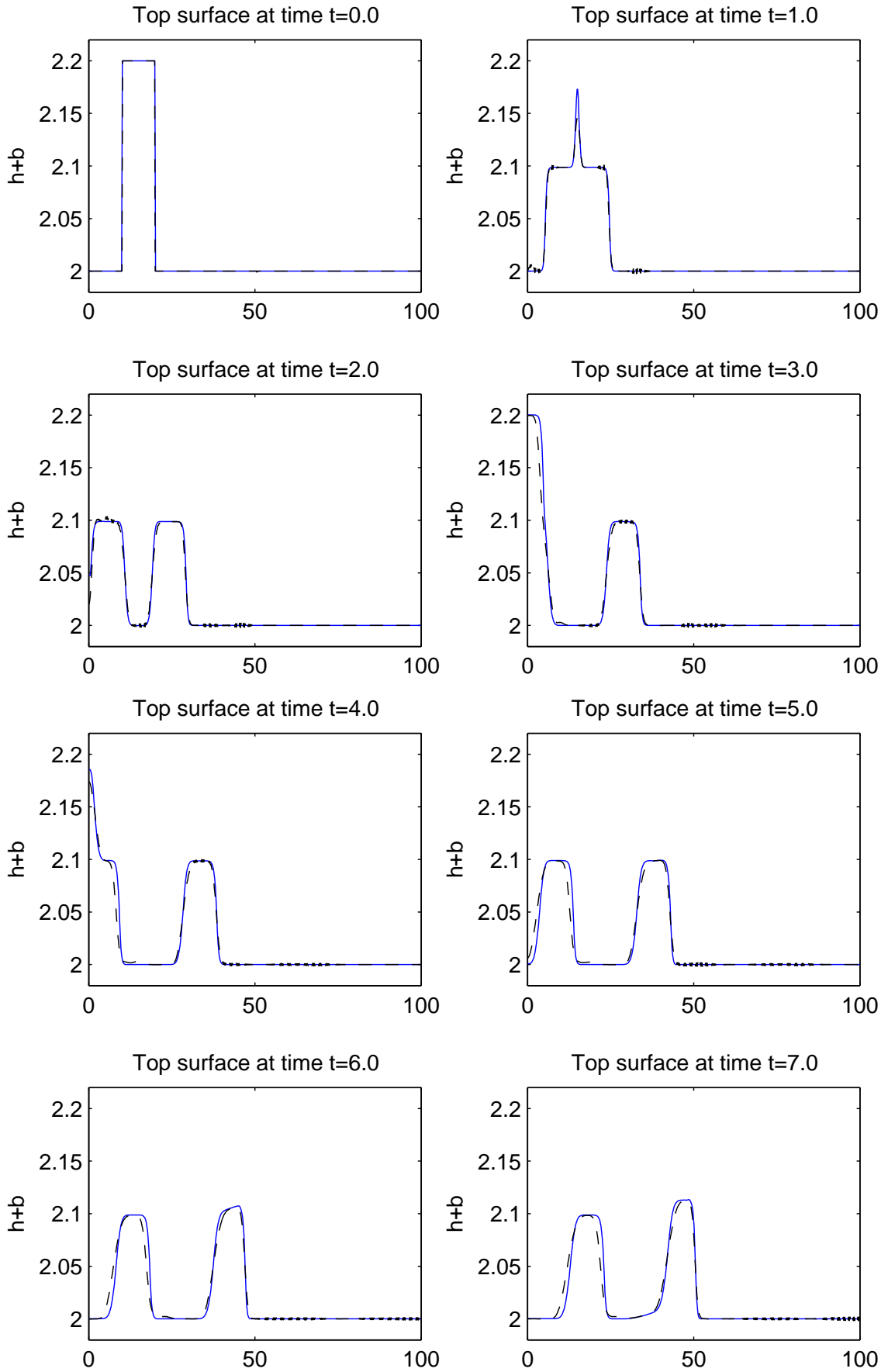


Figure 2: Propagation of small perturbations, $\varepsilon = 0.2$, $T = 0, 1, \dots, 7$ seconds; computed by the FVEG method (solid line) and by the FEM (dotted line).

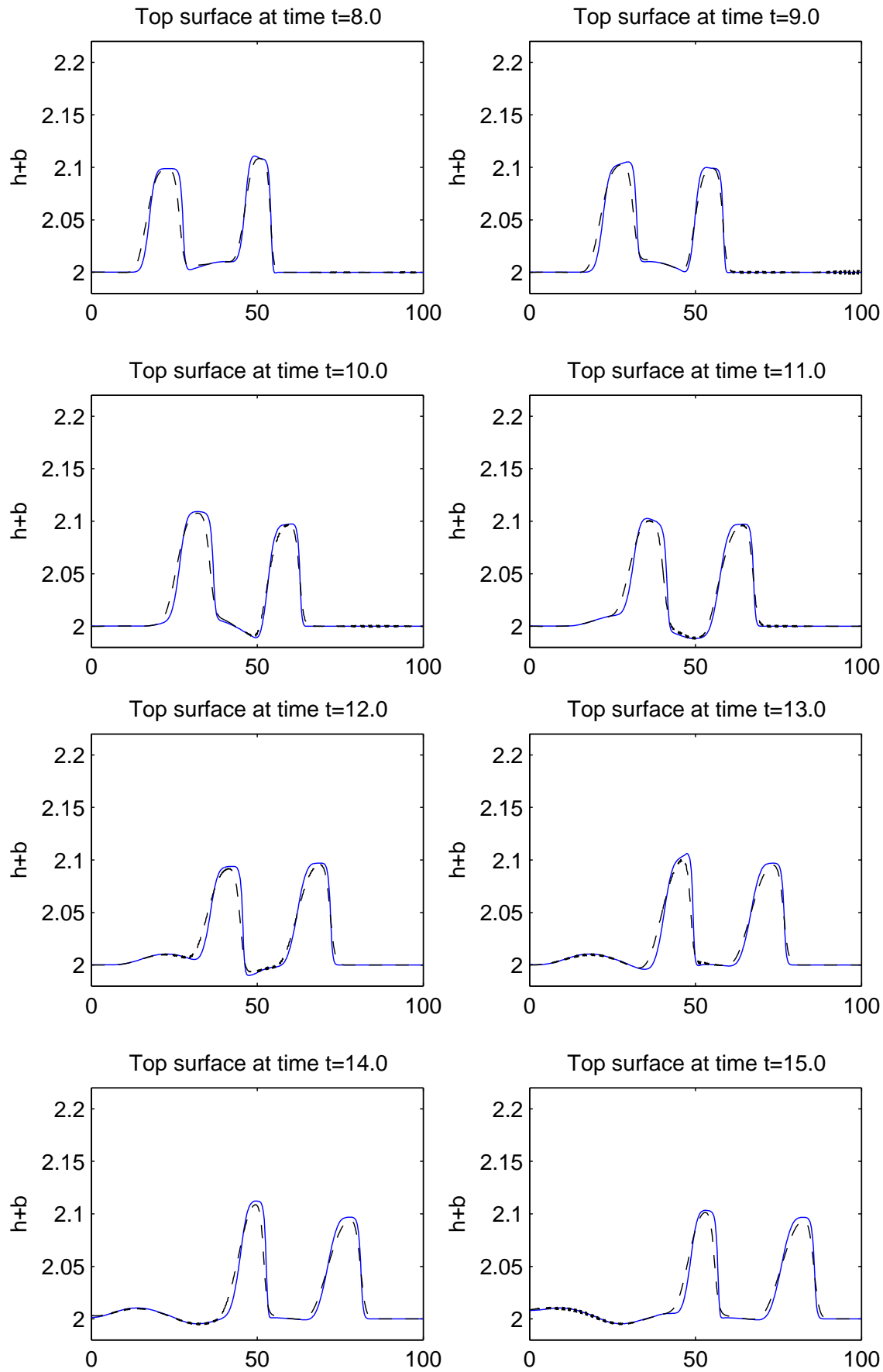


Figure 3: Propagation of small perturbations, $\varepsilon = 0.2$, $T = 8, 9, \dots, 15$ seconds; computed by the FVEG method (solid line) and by the FEM (dotted line).

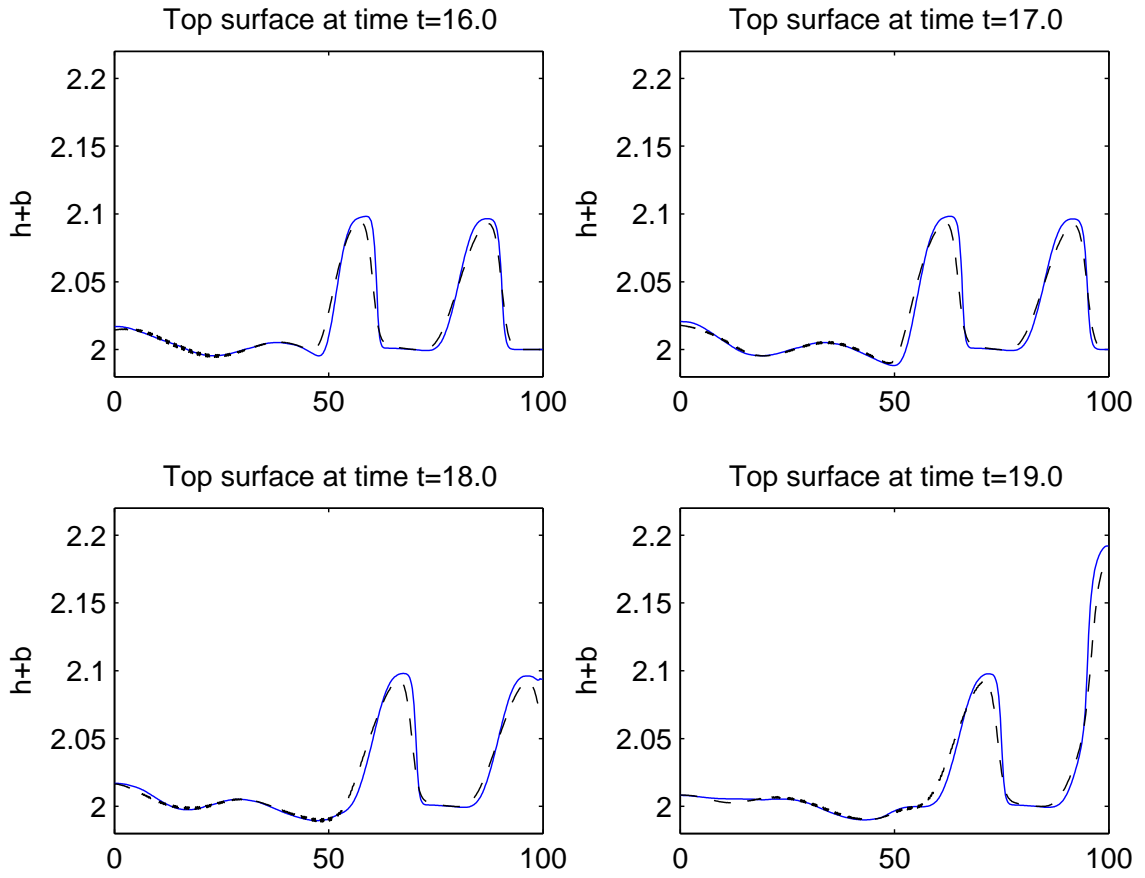


Figure 4: Propagation of small perturbations, $\varepsilon = 0.2$, $T = 16, 17, 18, 19$ seconds; computed by the FVEG method (solid line) and by the FEM (dotted line).

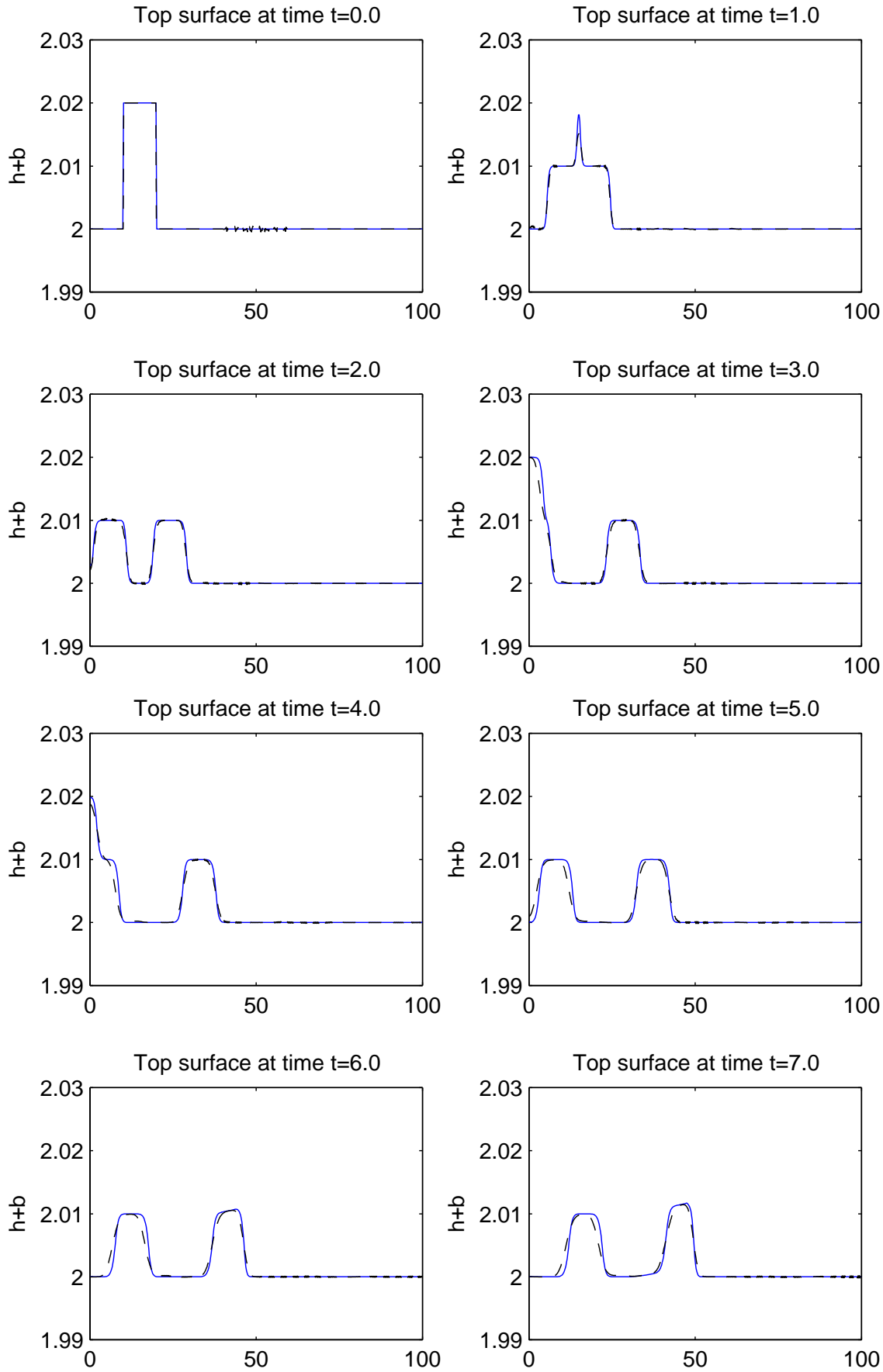


Figure 5: Propagation of small perturbations, $\varepsilon = 0.02$, $T = 0, 1, \dots, 7$ seconds; computed by the FVEG method (solid line) and by the FEM (dotted line).

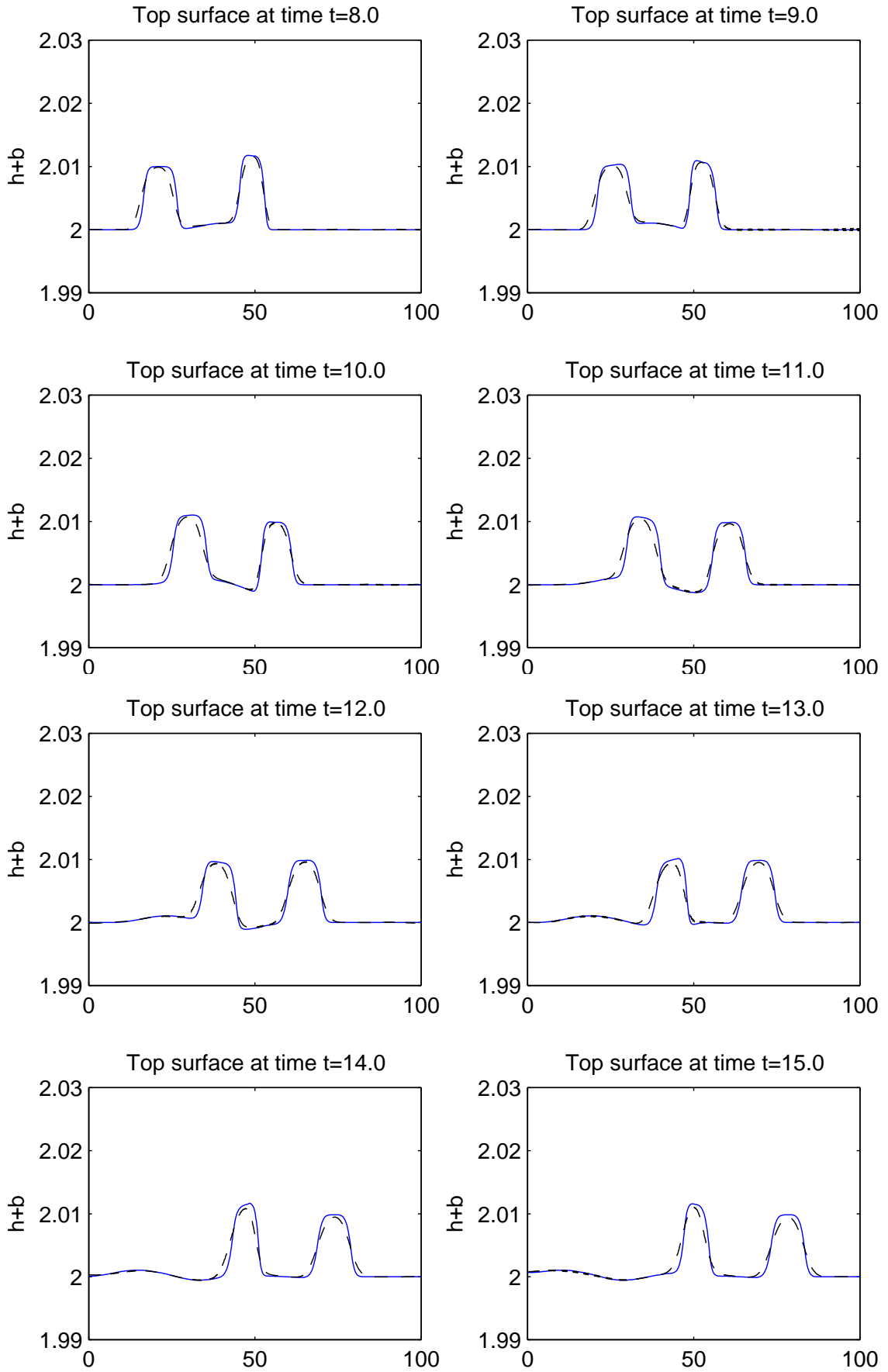


Figure 6: Propagation of small perturbations, $\varepsilon = 0.02$, $T = 8, 9, \dots, 15$ seconds; computed by the FVEG method (solid line) and by the FEM (dotted line).

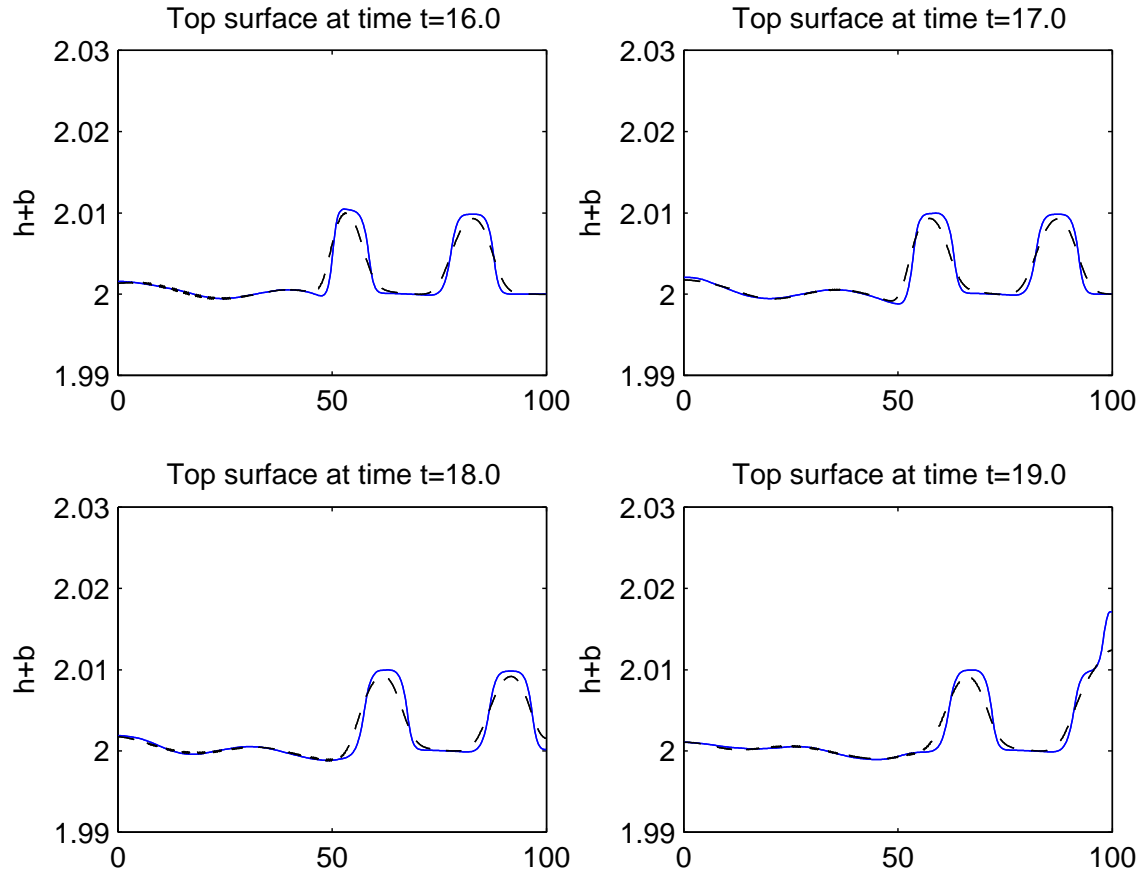


Figure 7: Propagation of small perturbations, $\varepsilon = 0.02$, $T = 16, 17, 18, 19$ seconds; computed by the FVEG method (solid line) and by the FEM (dotted line).

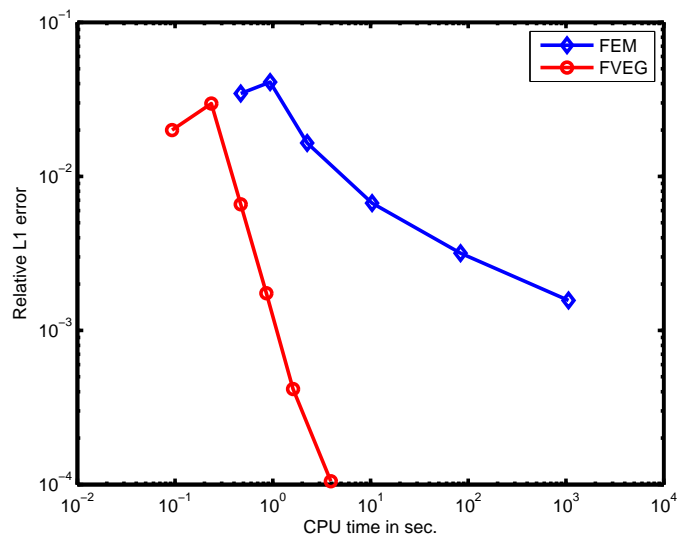


Figure 8: Efficiency test: relative L^1 error over CPU-time for the FVEG scheme (circles) and the FE method (boxes).